Prepared for the National Institutes of Health
National Institute of Neurological Disorders and Stroke
Division of Stroke, Trauma and Neurodegenerative Disorders
Neural Prosthesis Program
Bethesda, MD 20892

Microstimulation of the Lumbosacral Spinal Cord: Mapping

NIH-NINDS-NO1-NS-8-2300

Quarterly Progress Report #5

Period Covered: 1 October, 1999 - 31 December, 1999

Principal Investigator: Warren M. Grill, Ph.D.

Co-Investigators: Musa A. Haxiu, M.D., Ph.D.
Michel A. Lemay, Ph.D.

Department of Biomedical Engineering
Case Western Reserve University
Cleveland, OH 44106-4912

ABSTRACT

The objectives of this research are to determine the anatomical locations of spinal neurons involved in control of the genitourinary and hindlimb motor systems, and to determine the physiological responses evoked in the genitourinary and hindlimb motor systems by intraspinal microstimulation. During this quarter we made progress toward both of these objectives. We continued a series of experiments using immunocytochemistry to identify sacral spinal neurons than express the inhibitory neurotransmitter glycine. Secondly, we fabricated and characterized a 2 degree-of-freedom cartesian robot to characterize the hindlimb motor responses evoked by microstimulation of the lumbar spinal cord.

INTRODUCTION

Electrical stimulation of the nervous system is a means to restore function to individuals with neurological disorders. The objective of this project is to investigate the feasibility of neural prosthetics based on microstimulation of the spinal cord with penetrating electrodes. Specifically, chemical and viral retrograde tracers, immediate early gene expression, and immunocytochemistry are used to determine the locations and neurochemical identity of neurons in the spinal cord that control genitourinary and motor functions in the male cat. Microstimulation with penetrating activated iridium microelectrodes is used to determine the physiological effects in the genitourinary and motor systems of activation of different neural populations. The results of this project will provide data important to understanding neural control of genitourinary and motor functions, answer fundamental questions about microstimulation of the spinal cord, and lead to development of a new generation of neural prosthetics for individuals with neurological impairments.

PROGRESS IN THIS QUARTER

During the second quarter of this contract we continued a series of experiments using immunocytochemistry to identify sacral spinal neurons containing the inhibitory neurotransmitter glycine. We also fabricated and characterized a 2 degree-of-freedom cartesian robot that will be used to measure the hindlimb motor responses evoked by microstimulation of the lumbar spinal cord. Below each of our accomplishments is summarized.

Identification of Glycinergic Sacral Spinal Neurons

During reflex micturition the motoneurons innervating the external urethral sphincter are synaptically inhibited and pudendal afferent fibers receive presynaptic inhibition. The objective of these experiments is to identify inhibitory neurons that are active during reflex micturition. We have previously used patterns of c-Fos, the protein product of the immediate early gene c-fos, to identify spinal neurons active during reflex micturition in the male cat [Grill et al., 1998a], and used co-localization of c-Fos and parvalbumin [Grill et al., 1998b] and co-localization of the neurotransmitter gamma-amino butyric acid (GABA) to identify putative inhibitory neurons that are active during reflex micturition [QPR#1, NIH-NINDS-NO1-NS-8-2300]. The present experiments are designed to identify glycinergic neurons that are active during reflex micturition by co-localization of c-Fos and glycine. In the past quarter we focused our efforts on developing immunocytochemical methods for detection of glycine and spinal neurons.

METHODS

Immunocytochemistry was used to detect the presence of glycine in neurons in the lumbosacral spinal cord of cats. All animal care and experimental procedures were according to NIH guidelines and were reviewed and approved by the Institutional Animal Care and Use Committee of Case Western Reserve University. The details of the experimental preparation can be found in QPR. The animals were perfused via the aorta with saline followed by 4% paraformaldehyde in 0.1M $NaPO_4$ (pH=7.4). The brain and spinal cord were removed, stored in fixative for 2-5 days, and then transferred to 30% sucrose in 0.1M $NaPO_4$ (PBS) for 2-4 days. Tissue from these preliminary studies was taken from the lumbar segments, rather than from the sacral segments which are ultimately of interest.

Tissue Processing

The sacral spinal cord was sectioned transversely at 50 μm intervals on a freezing microtome and a 1 in 5 series of sections were processed for immunocytochemical detection of glycine. A summary of the primary antibodies, dilutions, secondary antibodies, and visualization methods tested is given in Table 5.1. Floating sections were rinsed in phosphate buffered saline (PBS), rinsed in PBS containing 0.3% Triton X-100 for 1 h, and then exposed to primary antibody against glycine (Chemicon, Alpha Diagnostics, Strategic Biosolutions, see Table 5.1) in a blocking solution of PBS/Triton/BSA 1% overnight on a shaker at 4 degrees with dilutions ranging from 1:100-1:500. Sections were then washed in PBS/Triton 3X for 5 minutes. Next, the sections were exposed to an appropriate biotinylated secondary antibodies (Table 5.1) in

a blocking solution of PBS/Triton/BSA for 1-4 hrs at room temperature at a dilution of 1:200. Sections were washed with PBS 2X for 10 minutes and processed using a standard biotin avidin peroxidase kit (ABC Elite, Vector Laboratories, Burlingame, CA) at 5ul/ml in PBS for 1hr at room temperature. Sections were washed in PBS 3X for 5 minutes and placed in a DAB solution (Sigma) either with or without nickel chloride enhancement for 30-90 seconds. Sections were then washed 2X in ddH2O for 5 minutes and 1X in PBS, mounted on gelatin coated slides, air dried, dehydrated in ascending concentrations of alcohol from 70%-100%, coverslipped with Paramount mounting medium and viewed with a light microscope.

Primary Antibody	Dilution	Secondary Antibody	Method	Cat #
Alpha Diagnostics	1:100, 1:200,	*Jackson Labs*	ABC	528-L6,L7
mouse anti glycine	1:300,1:400,	Biotin-Donkey anti-Mouse	ABC + NiCl	536-L5,L6,L7
	1:500	1:200		549-L7
Strategic Biosolutions	1:100, 1:200,	*Jackson Labs*	ABC	528-L6
goat anti glycine	1:300,1:400,	Biotin-Donkey anti-Goat	ABC + NiCl	536-L7
	1:500	1:200	TRITC	549-L7
Chemicon	1:100, 1:200,	*Jackson Labs*	ABC	528-L6
rabbit anti glycine	1:300,1:400,	Biotin-Donkey anti-Rabbit	ABC + NiCl	536-L7
	1:500	1:200		549-L7

Table 5.1 Summary of immunocytochemical methods tested for detection of glycine in cat spinal neurons.

RESULTS AND DISCUSSION

Although we tried a large number of combinations of antibodies and dilution we did not obtain reliable labeling of glycine in spinal neurons. We did see occasionally labeled neurons as well as labeled fibers, but the intensity and repeatability of labeling was unsatisfactory.

It has been established that fixatives containing aldehyde can mask antigens (e.g., glycine) by protein crosslinking and/or protein denaturation [Fox et al., 1985, Dapson, 1993] or by complexing of hydromethyl groups between neighboring proteins [Morgan et al., 1997]. As this tissue was fixed with paraformaldehyde this may explain the poor labeling that we observed. In the next quarter we will use heating and calcium chelation to try to improve glycine antigenicity [Jiao et al., 1999].

Planar Manipulator for Characterization of Cat Hindlimb Mechanical Properties

Our on-going investigation of the cats hindlimb motor response to intraspinal microstimulation has revealed that patterns of forces, termed force fields (FF), are produced. The force fields are of a set of vectors, each plotted at the limb position at which it was measured, with vector length proportional to force magnitude and vector direction representing force orientation. Thus far our measurements have been made under isometric conditions. To expand our investigation to movement conditions, we designed, assembled, and began characterization of a two degree-of-freedom cartesian robot suited to measure the mechanical properties of the feline's hindlimb in the sagittal plane. The manipulator was designed to provide two primary functions: the ability the record the movement produced by intraspinal stimulation, and the ability to impose controlled forces on the limb while simultaneously recording the resulting movement and reaction forces. The manipulator can be used under a wide range of loading conditions: from isometric during measurements of the forces to free-moving during measurement of the motion.

Robotic System Architecture

A diagram of the overall system is shown in Figure 5.1. The manipulandum is a parallelogram mechanism that allows direct drive of each of the joints. One motor controls the inner or shoulder joint, while the other motor controls the outer or elbow joint. Rotary position is sensed via encoders, and a three-dimensional force/moment transducer measures the forces applied to the end-point (to which the cat's paw will be attached). The position and force information are stored/processed by a computer that also produces the desired motor command. Power is supplied to the motors via two power amplifiers that convert the command voltage to a controlled current. The following sections will examine each of the assembly components separately.

Manipulandum

The linkages are assembled in a four bar configuration (Figure 5.2) which permits direct drive of each of the two joints (shoulder and elbow). This eliminates the cross-coupling between joints inherent in cable-driven systems, and the slippage/friction introduced by gear/pulley systems. Motion is in the plane perpendicular to the motor/joint axis, and the kinematics of the linkage are defined by the following equations:

$$x = L_1 \cos(\theta_S) + L_2 \cos(\theta_S + \theta_E)$$

$$y = L_1 \sin(\theta_S) + L_2 \sin(\theta_S + \theta_E),$$

where x, y are the end-point Cartesian coordinates, L_1 and L_2 are the lengths of the inner and outer links respectively, and θ_S and θ_E are respectively the shoulder and elbow angles. Since the linkages can not fold unto themselves or fully extend (elbow joint

motion is from 10° to 150° in relative angle, i.e. with respect to the shoulder linkage), the mechanism can not reach singular configurations, and the inverse kinematics are unambiguously defined by:

$$\theta_S = \text{atan2}(y,x) - \text{atan2}(\kappa, x_2 + y_2 + L_1^2 - L_2^2)$$

$$\theta_E = \text{atan2}(\kappa, x^2 + y^2 - L_1^2 - L_2^2)$$

$$\kappa = \sqrt{(x^2 + y^2 + L_1^2 + L_2^2)^2 - 2\left[(x^2 + y^2)^2 + L_1^4 + L_2^4\right]}.$$

The actual physical dimensions in our case are:

L_1=11.43 cm : distance from the center of the motor shaft controlling shoulder motion to the center of rotation of the elbow.

L_2=10.45 cm : distance from the elbow center of rotation to the force sensor z- axis (i.e., the axis perpendicular to the robot's plane of motion).

Position is sensed by measuring the rotation of each motor shaft via an encoder attached to the rear extension of the shaft. Encoders are optical with a resolution of 625 lines/revolution. The encoder also presents an index for absolute reference positioning. Encoder resolution is augmented to 320,000 pulses/revolution via a 128X interpolator, and quadrature multiplication on the PC installed counter card. This provides an angular resolution of 0.001125° which corresponds to ≈0.002 mm of end-point resolution.

The end-point forces developed by the motors are easily calculated using the Jacobian of the kinematic linkage:

$$F = (J^T)^{-1}\tau$$

$$J = \begin{bmatrix} -L_1 \sin\theta_S - L_2 \sin(\theta_S + \theta_E) & -L_2 \sin(\theta_S + \theta_E) \\ L_1 \cos\theta_S + L_2 \cos(\theta_S + \theta_E) & L_2 \cos(\theta_S + \theta_E) \end{bmatrix}$$

Since the mechanism can not reach singular configurations, the Jacobian J is invertible and the end-point forces can be calculated throughout the workspace. The motors used can develop 2.3 N•m (at 20A, which the amplifiers can deliver for 2s). In the middle of the workspace this corresponds to force levels of approximately 18N.

Robot Amplifier Assembly

The robot amplifier assembly houses the two linear amplifiers used to drive the motors. Linear voltage controlled current amplifiers were chosen to avoid the electromagnetic noise caused by pulse-modulated amplifiers. Maximum continuous current is 5A (2A/V), with peak current of 20A for 2 seconds. The motors can be disabled using a TTL input (enable0 and enable1 in Figure 5.3), or from a large emergency off button which simultaneously disconnects the power to both motors. The current sense output provides a voltage level representative of the current applied to the motors (0.1V/A). Further details on the functioning of the amplifiers can be found in the

amplifier's user manual (publication EDA105 from Aerotech Inc., see the part list section for more information).

Computer Interface & Encoder Circuitry Assembly

The computer interface & encoder circuitry assembly (Figure 5.4) serves two functions: 1) it provides an interface between various external signals (force sensor, EMGs, motor command, etc.) and the computer's data acquisition board, and 2) it houses the encoder interpolator circuitry. The various signals of the computer data acquisition board are connected via two 50 pin ribbon cables to two interconnect boards mounted inside the assembly cabinet. These boards are connected to multiple BNC connectors mounted on the face panel of the cabinet. These BNC provide an interface between the outside world, and the control software of the computer. The cabinet also houses two interpolator boxes that increase the resolution of the encoders by a factor of 128. The interpolated pulses are then connected into a counter card mounted inside the computer. Finally, some electronic circuitry is used to clock the data acquisition board's counters, which are used to generate the timing for electrical stimulation pulses.

The card's counters are based on the industry standard 82C54 chip. The three available user counters are programmed to generate TTL pulse train used to drive a current controlled microstimulator. A pulse train is initiated by a rising edge on the gate of counter 4. This initiates the counter which determines the duration of the train. The output of the counter serves as a gating signal for counter 5, which generates pulses at the clock/counter frequency on its output. Those pulses are used as triggers for counter 6, which is programmed as counter 4 to produce pulses of a fixed duration. The train durations achievable are from 0-4.096 sec ($(2^{16}-1)/16{,}000$), stimulation frequency from 0.244 -16,000 Hz (clock is 16KHz, see Figure 5.5), and pulse duration from 0-6.554 ms in 0.1μsec increments (counter 6 uses a 10MHz internal clock). Stimulation is initiated by using one of the data acquisition card's digital outputs as the input to the gate of counter 4.

Characterization of the Robot's Capabilities

In addition to designing and assembling the robotic system, we have characterized the electro-mechanical performance of the design. We evaluated the manipulandum's range of motion, the ability to produce forces in all directions, and the frequency response of the system.

The manipulandum's range of motion is presented in Figure 5.6 in relation to an average size cat's hindlimb. The robot's range of motion is approximately 23 by 11 cm which is sufficient to cover the region explored in our microstimulation study (9 by 9 cm). This range of motion would also be appropriate to measure the kinematics of the hindlimb during normal walking.

The force capabilities at the end-point are presented in Figure 5.7. The figure shows a rotating force vector produced at a central location in the workspace. The figure was produced by commanding the robot to produce low frequency (0.33 Hz) sinusoidal forces in the x and y Cartesian directions. The circles are drawn by plotting the y forces (cosine) *versus* the x forces (sine), and they illustrate the ability of the motors to produce a constant force vector in any directions from the center of the circle. The force range investigated was from 1-10N, and the theoretical capacity of the motor/amplifier should be 18N (for periods of up to 2 seconds). We know from our previous measurements of isometric forces during intraspinal microstimulation that levels of 10N should be sufficient for our studies.

The robot's frequency response is presented in Figure 5.8. The magnitude response was obtained by commanding a sinusoidaly varying 2N endpoint force in the x or y direction, while the force in the other direction was commanded to zero. The sinusoidal frequency was linearly increased from 0 to 100Hz in 100sec, and the forces produced at the end-point were recorded. The figure demonstrates that the magnitude response of the robot is flat to 100Hz, which is significantly above the maximal 3Hz frequency of human or animal movements. Further, these data demonstrate minimal cross coupling between forces commanded in one direction (x in upper panel, y in middle panel) and off axis force production. While the magnitude response of the robot was relatively flat, the phase lag increased with frequency (see bottom panel of Figure 5.8). For the range of frequencies encountered during motion the phase lag is sufficiently small ($<10°$) not to cause instability problems.

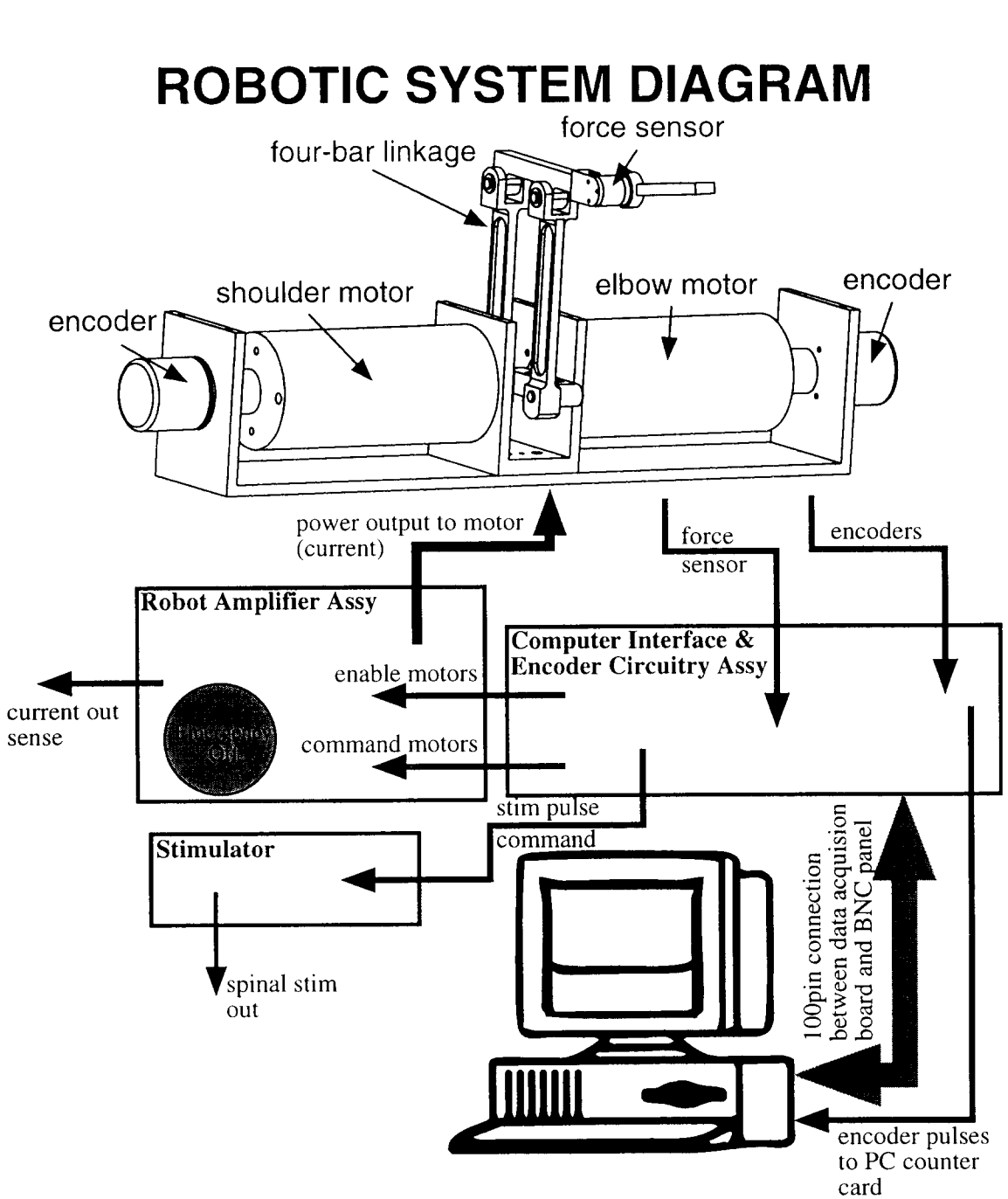

Figure 5.1. Diagram of the 2 degree-of-freedom Cartesian robot system. The kinematic linkage and motor assembly are shown at the top. Robot movement is in the vertical plane, which corresponds to the animal's sagittal plane when it is mounted in a stereotaxic frame. Position is sensed by optical encoders attached to the motors' rear shaft. Endpoint force is sensed by a commercial three-axis force/moment transducer mounted at the end of the outer linkage. A gimbal, to which the paw is attached, is mounted on the force transducer, and allows the rotation of the ankle joint that occurs as the limb is moved. Outside information is passed to and from the PC data acquisition board (DAQ) via the Computer Interface & Encoder Circuitry Assembly. The encoder signal is the only information that is not processed by the DAQ, and is instead fed into a counter card mounted inside the computer. Digital to analog outputs from the DAQ board are used to control amplifiers supplying current to the motors (Robot Amplifier Assembly). Three counters on the DAQ board are used to generate a TTL pulse train that drives a current controlled stimulator.

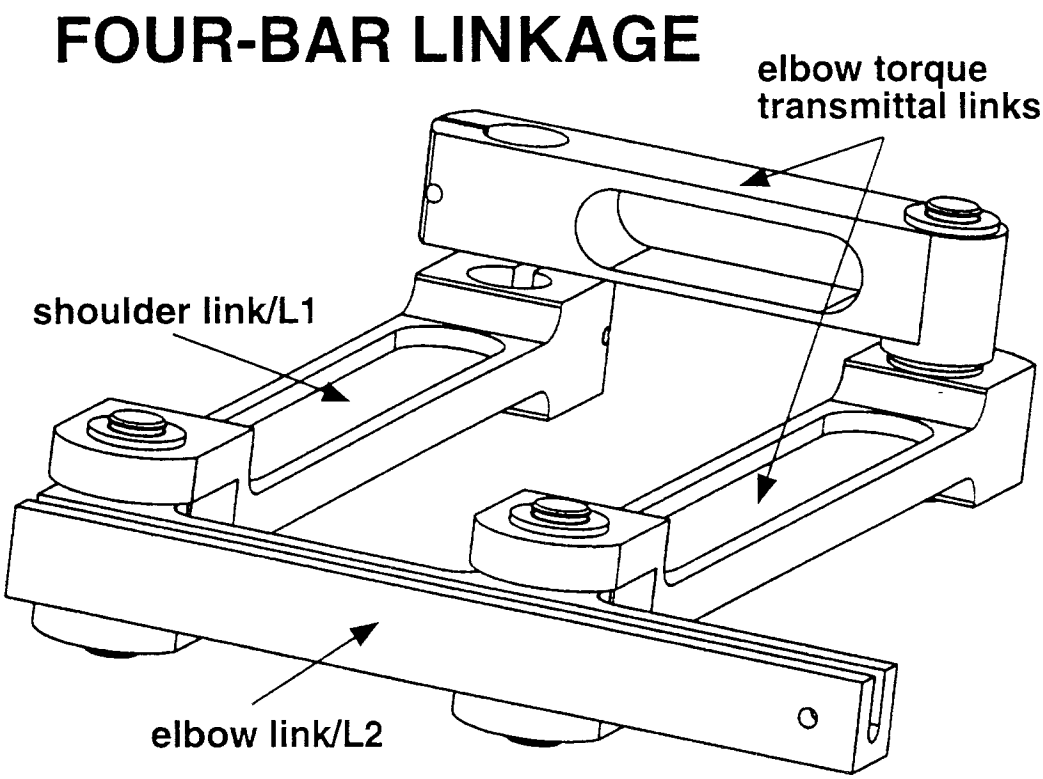

Figure 5.2. Details of the four bar linkage assembly. The parallelogram design permits direct drive of each joint which simplifies the robotic control, and eliminates the complex dynamic effects introduced by the friction/slippage of gear/pulley systems. The links are made of aircraft quality Aluminum (7075 Al) to maximize the stiffness to weight ratio. Two high-quality (ABEC-5) bearings are used at each joint to minimize rotational friction and the lateral play of the joint. Cut-outs further reduce the links' weight, and the groove in the elbow link is used as a conduit for the force sensor cable.

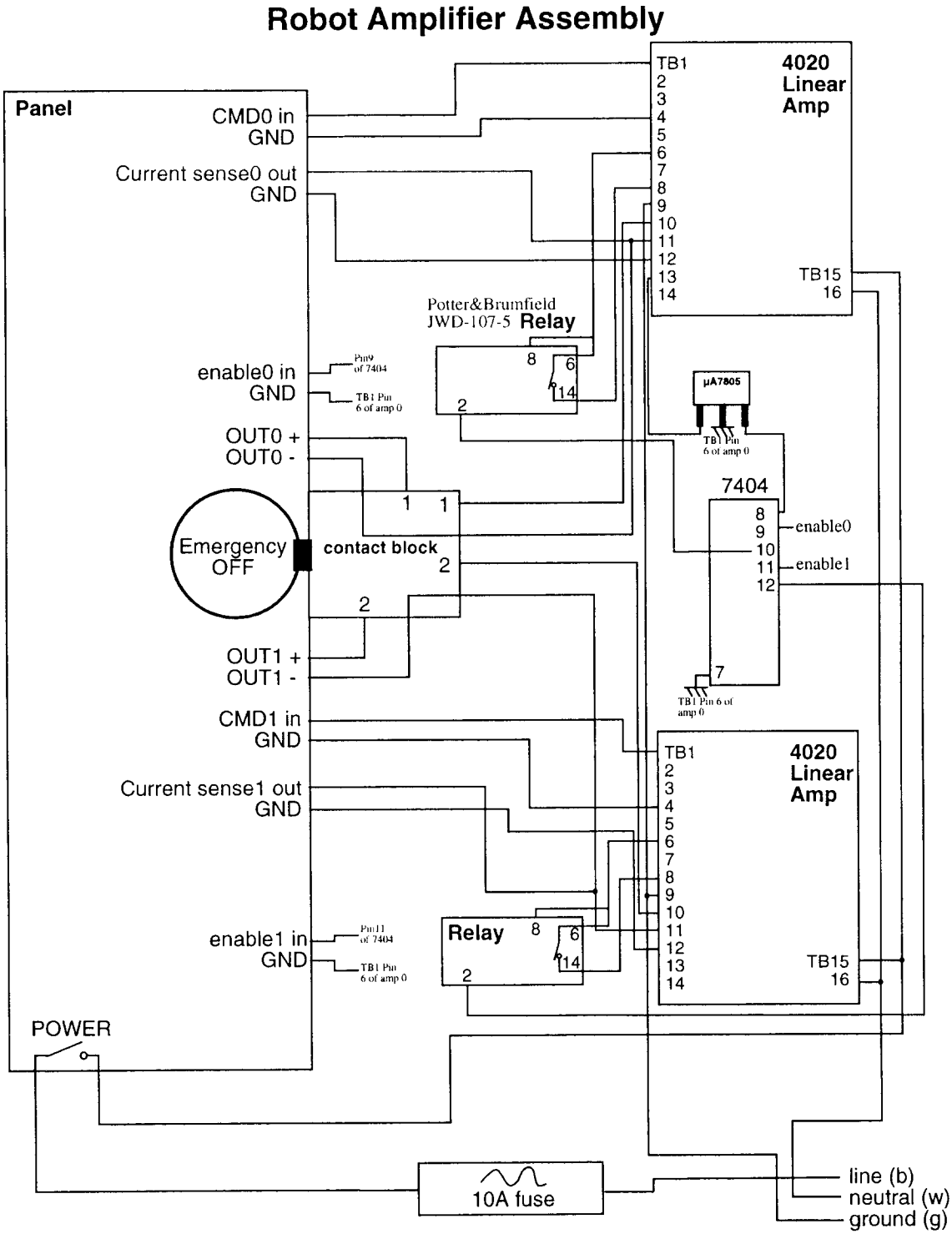

Figure 5.3. Schematic of the Robot Amplifier Assembly. This diagram with the associated parts list describes the components and wiring of the assembly. The linear amplifiers are set to operate in current control mode (2A/V) under a voltage command (CMD). The motor output (OUT) can be disconnected by the Emergency OFF button, or disabled by a low level on the enable input (enable high, i.e. 5V enables current through the motors). The output current can be measured as a voltage present on the current sense output (0.1V/A).

Computer Interface & Encoder Circuitry Assy

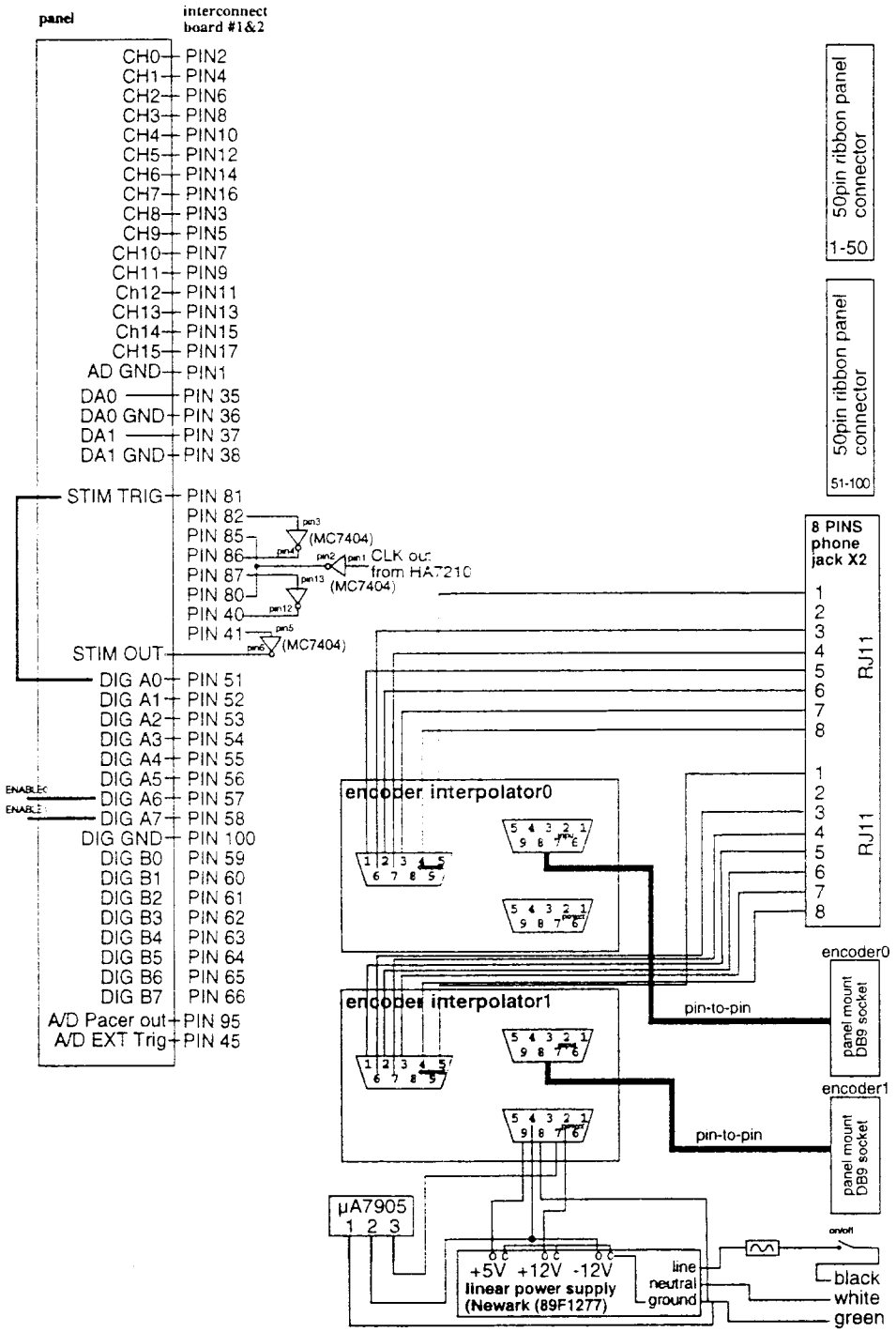

Figure 5.4. Schematic of the Computer Interface & Encoder Circuitry Assembly. This diagram with the associated parts list describes the components and wiring of the assembly. The encoder interpolators are powered from a low-noise linear power supply. The raw encoder analog signals are fed directly into the interpolators and the output pulses are then routed out via 2 RJ11 connectors. Those connect to a counter card inside the computer using shielded phone cables. The computer data acquisition board (DAQ) is connected in the cabinet's back panel via two 50 pin ribbon cable connectors that attach to two interconnect boards. Those boards are wired to BNC connectors mounted on the front panel of the cabinet (left side of the diagram). Analog to digital channels are marked CH0-15, digital to analog channels are marked DA0-1, and the digital input/output lines are marked DIG A0-7 & DIG B0-7. A clock circuit is provided for the counters of the DAQ card. Those counters are used to generate TTL pulse train that drives a stimulator. STIM TRIG triggers the onset of the programmable pulse train, and STIM OUT is the TTL output used to drive the stimulator.

Clock Circuit

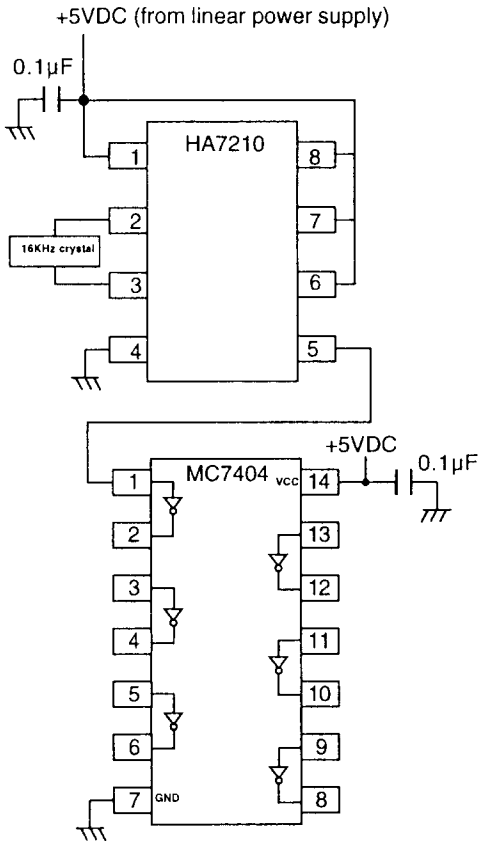

Figure 5.5. Clock circuit used to drive the clock of the data acquisition board user counters 4 & 5 (ComputerBoards Inc. PCI-DAS1002). This clock circuitry is mounted inside the Computer Interface & Encoder Circuitry cabinet. The clock is based on an Harris 7210 (Harris Corporation, http://www.semi.harris.com). The only required external component is the clock crystal. The crystal chosen is a 16KHz crystal. The clock output is fed into an hex inverter (MC7404) that is also used to invert some of the counters' outputs and gates (see schematic of the Computer Interface & Encoder Circuitry Assembly).

Parts Lists for All Assemblies

TABLE I - Amplifier Assembly (fig. 3) Parts List

Parts	**Manufacturer/supplier**	*Qty*
cabinet	Newark Electronics part # 99F1014	1
amplifier	Aerotech Inc. part # 4020C-LS-A-F5	2
relay	Newark Electronics part # 81F9287	2
inverter	MC7404 (in-house stock)	1
DC converter	µA7805 (in-house stock)	1
emergency off	Newark Electronics part # 50F7339	1
BNC panel	Newark Electronics part # 93F7577	6
Motor connector	Newark Electronics part # 89F4127 (panel mount) Newark Electronics part # 89F4108 (cable end)	2 2
Al fan cover	Newark Electronics part # 87F3918 Newark Electronics part # 87F3928	2 2
emergency off contact block	Newark Electronics part # 50F7321	1

TABLE II - Computer Interface and Encoder Circuitry Assembly (fig. 4) Parts List

Parts	**Manufacturer/supplier**	*Qty*
encoder interpolator	Dynamics Research Corporation part # ER128A-NC16	2
interconnect board	ComputerBoards Inc. part # CIO-MINI50	2
linear power supply	Newark Electronics part # 89F1277	1
RJ11 phone jacks	Newark Electronics part # 95F1472	1
BNC panel	Newark Electronics part # 93F7577	38
50 pins ribbon cable panel connector	Newark Electronics part # 87F3976 (socket) Newark Electronics part # 87F4010 (strain relief) Newark Electronics part # 94F3335 (latches)	2 2 4
50 pins ribbon cable connector	Newark Electronics part # 46F8395 (socket) Newark Electronics part # 46F4673 (strain relief)	2 2
DB9 sockets	Newark Electronics part # 89F1461 (socket panel mount) Newark Electronics part # 44F8774 (post)	2 2
DB9 pins	Newark Electronics part # 89F1466	4
DB9 shell	Newark Electronics part # 89F001	6
µA7905	Newark Electronics part # 07F7753	1
switch	in-house stock	1
fuse holder	in-house stock	1

fan	Newark Electronics part # 46F5099	1
fan cover	Newark Electronics part # 87F3920	1
Al fan cover	Newark Electronics part # 87F3928	1
clock	Harris Semiconductor HA7210 (in-house stock)	1
16Khz crystal	Golledge Electronics Limited part # CC1V 16Khz	1
hex inverter	MC7404 (in-house stock)	1
capacitor	0.1μF (in-house stock)	1
cabinet	Newark Electronics part # 99F1013	1
encoder cable	US Digital Corporation part # CA-SH8-MD8-MD8-6FT	2

TABLE III - Robot Assembly Major Components

Parts	**Manufacturer/supplier**	*Qty*
motors	Cleveland Motion Controls part # 2630000MT000TAA-B0	2
rotary encoder	Dynamics Research Corporation part # S1524E3649625	2
force sensor	ATI Industrial Automation part # Nano 25/250	1
flexible interconnect	Helical Products part # AR100-12-8	2

TABLE IV - Computer Cards

Parts	**Manufacturer/supplier**	*Qty*
counter card	US Digital Corporation part # PC7266-D	1
data acquisition board	ComputerBoards Inc. part # PCI-DAS1002	1

Suppliers and manufacturers:

Cleveland Motion Controls
829A Middlesex Turnpike
Billerica, MA 01821-3954
www.cmccontrols.com

Aerotech Inc.
101 Zeta Drive
Pittsburgh, PA 15238
www.aerotechinc.com

Helical Products
901 W. McCoy Lane
Santa Maria, CA 93455
www.Heli-Cal.com

US Digital Corporation
3800 N.E. 68th St. #A3
Vancouver, WA 98661
www.usdigital.com

Newark Electronics
4614 Prospect Av.
Cleveland, OH 44103-3780
www.newark.com

Dynamics Research Corporation
60 Concord St.
Wilmington, MA 01887-2193
www.drc.com

ComputerBoards Inc.
16 Commerce Blvd.
Middleboro, MA 02346
www.computerboards.com

Golledge Electronics Limited
Ashwell Park • Ilminster
Somerset TA19 9DX, UK
www.golledge.co.uk

ATI Industrial Automation
Peachtree Ctr, 503-D Highway 70 East
Garner, NC 27529
www.ati-ia.com

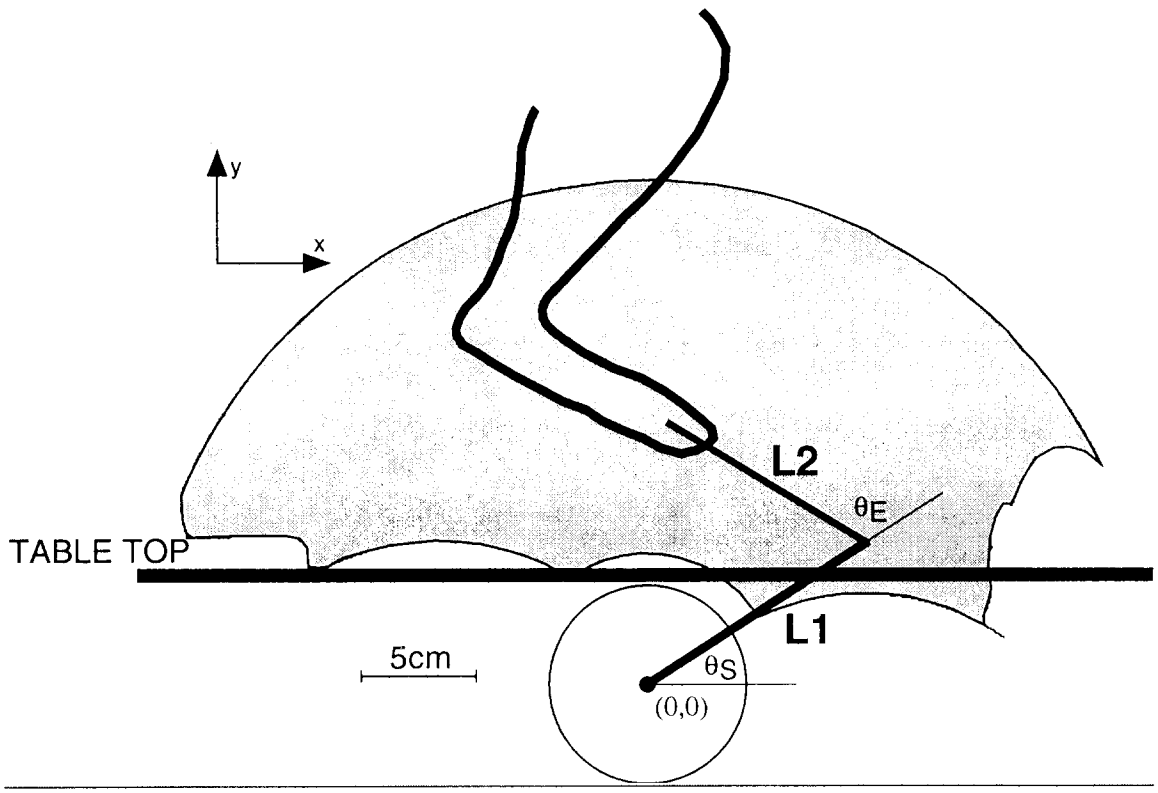

Figure 5.6. Manipulandum's range-of-motion. The diagram shows the location of the manipulandum's motors with respect to the experimental table. The motors are mounted underneath the stereotaxic frame's table, and the links protrude through a slot in the table top. The usable range-of-motion is approximately 23 by 11 cm (23 cm horizontally, 11 cm vertically). This covers the range used until now to measure isometric force fields, and spans the cat's range of motion during walking. The dimensions for L1 and L2 are respectively 11.43 cm and 10.45 cm.

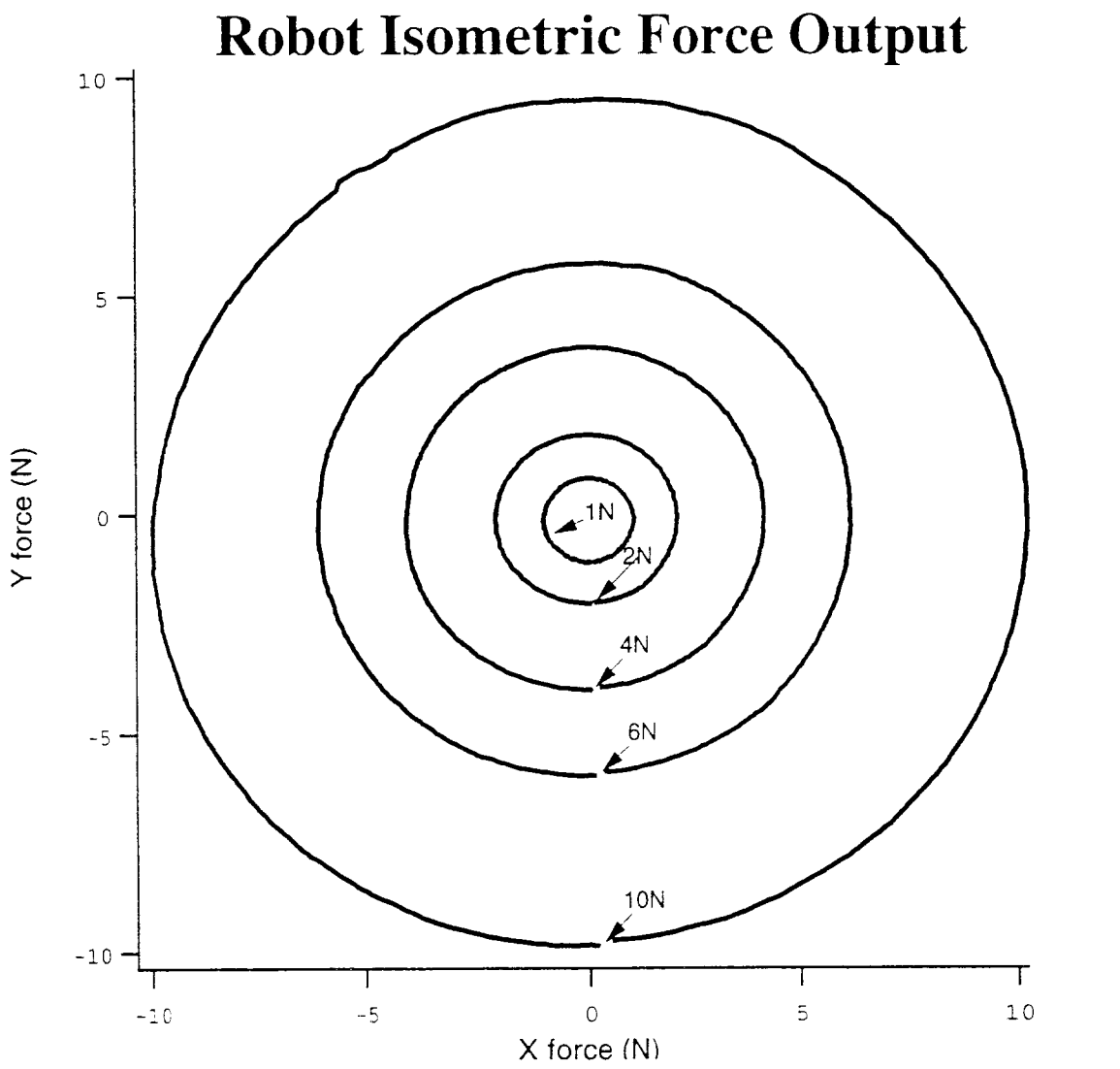

Figure 5.7. Rotating force vector produced at the robot's end-point while it is being held isometrically in the center of the workspace. The command to the robot was to produce sinusoidal forces of 5 different amplitudes in the x and y directions. The plotted curves are the actual forces in y (cosine function) plotted *versus* the forces in x (sine function) for the 5 amplitudes: 1N, 2N, 4N, 6N, and 10N. The graph demonstrates the robot's ability to produce a desired force level in any direction.

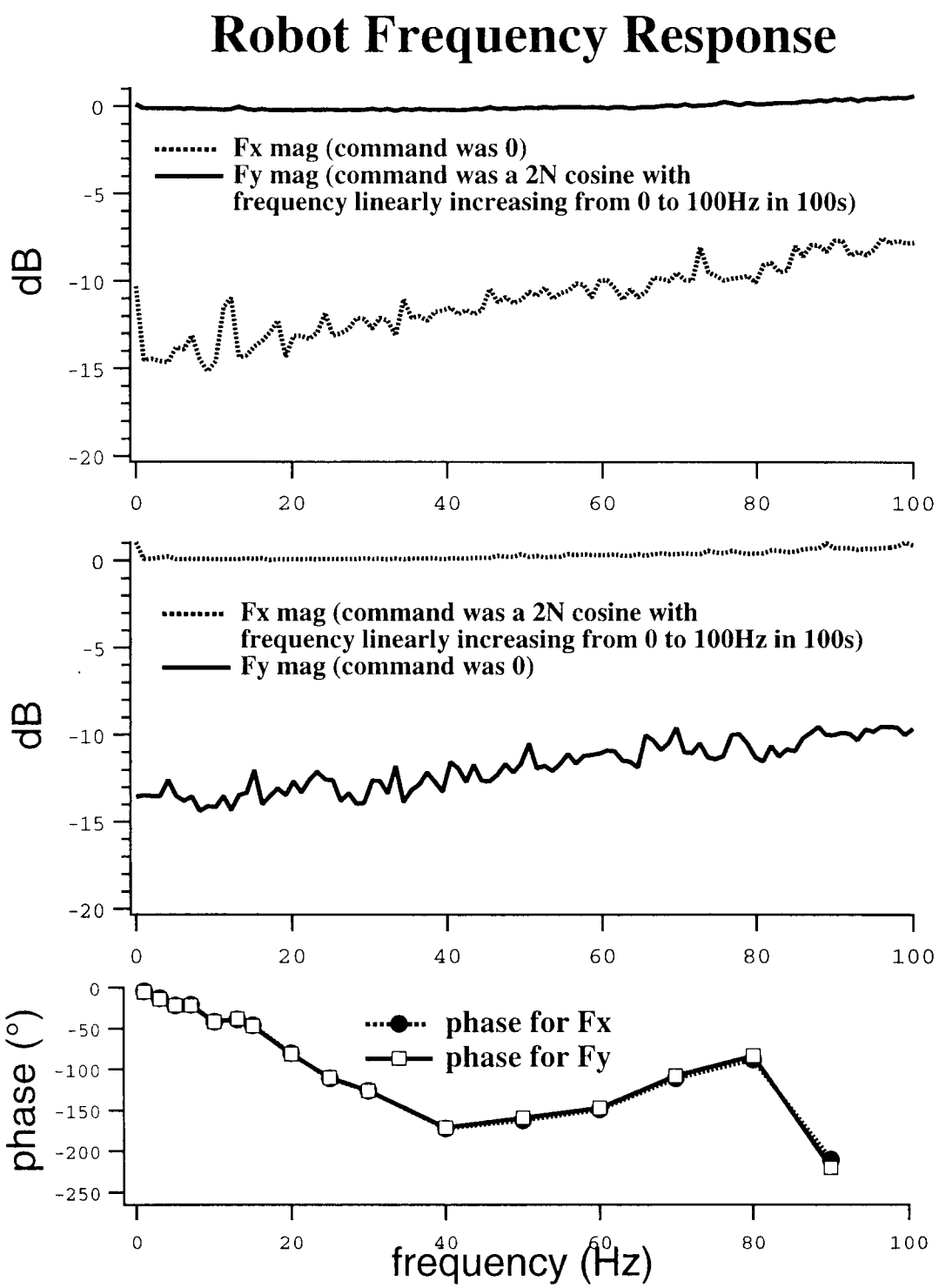

Figure 5.8. Magnitude and phase response of the robot to commanded Cartesian forces. The two top panels were obtained by inputing a 2N sinusoidal command with linearly increasing frequency for one direction (y on the top panel, x on the middle panel) while the other direction's command was zero. The results show that the magnitude response is flat to about 100Hz, and that cross-coupling to the perpendicular direction is limited. The phase response (bottom panel) was obtained by inputting fixed frequency sinusoidal commands to both directions simultaneously (since we showed that they are decoupled), and measuring the resulting phase differences between command and output. The phase lag increases with frequency but is relatively small (<10°) in the frequency range of interest (0-5Hz).

PUBLICATIONS THIS QUARTER

Lemay, M.A., W.M. Grill (1999) Endpoint forces evoked by microstimulation of the cat spinal cord. Proc. 21st Ann. Int. Conf. IEEE-EMBS.

Lemay, M.A., W.M. Grill (1999) Spinal force fields in the cat spinal cord. Society for Neuroscience Abstracts 25:1396.

OBJECTIVES FOR THE NEXT QUARTER

In the next quarter we will continue our co-localization studies to identify inhibitory spinal neurons active during micturition. Specifically, we will explore heating and calcium chelation to restore glycinergic antigenicity in paraformaldehyde fixed tissue [Jiao et al., 1999].

We will continue our studies characterizing the hindlimb motor responses to lumbar microstimulation. Our specific objectives are to complete characterization of the two degree-of-freedom robot, and to resume experiments measuring the hindlimb motor responses evoked by microstimulation of the lumbar spinal cord.

Finally, we will continue development of our electrical mapping method [see QPR#4, NIH-NINDS-NO1-NS-8-3200]. Our specific objective is to study the influence of the electrical properties of the volume conductor (inhomogeneity, anisotropy) on the surface potentials produced by intraspinal sources.

LITERATURE CITED

Dapson, R.W. (1993) Fixation in the 1990s: a review of needs and accomplishments. Biotechnol. Histochem. 68:75-82.

Fox, C.H., F.B. Johnson, J. Whiting, P.P. Roller (1985) Formaldehyde fixation. J. Hisotchem. Cytochem. 33:845-53.

Grill, W.M., B. Wang, S. Hadziefendic, M.A. Haxhiu (1998a) Identification of the spinal neural network involved in coordination of micturition in the male cat. Brain Research 796:150-160.

Grill, W.M., S. Hadziefendic, B.O. Erokwu, M.A. Haxhiu (1998b) Co-localization of parvalbumin and c-fos in sacral spinal neurons involved in regulation of micturition. Society for Neuroscience Abstracts 24:1618.

Jiao, Y., Z. Sun, T. Lee, F.R. Fusco, T.D. Kimble, C.A. Meade, S. Cuthbertson, A. Reiner (1999) A simple and sensitive antigen retrieval method for free-floating and slide-mounted tissue sections. J. Neurosci. Methods 93:149-162.

Morgan, J.M., H. Navabi, B. Jasani (1997) Role of calcium chelation in high-temperature antigen retrieval at different pH values. J. Pathol. 182:233-237.